High-temperature Thermoelectric Properties of Ca0.9Y0.1Mn1-xFexO3 (0 x 0.25)

Le, Thanh Hung; Van Nong, Ngo; Han, Li; Minh, Dang Le; Borup, Kasper A.; Iversen, Bo B.; Pryds, Nini; Linderoth, Søren

Published in:
Journal of Materials Science

Link to article, DOI:
10.1007/s10853-012-6834-z

Publication date:
2013

J Mater Sci
DOI 10.1007/s10853-012-6834-z

ENERGY MATERIALS & THERMOELECTRICS

High-temperature thermoelectric properties of $Ca_{0.9}Y_{0.1}Mn_{1-x}Fe_xO_3$ ($0 \le x \le 0.25$)

Le Thanh Hung · Ngo Van Nong · Li Han · Dang Le Minh · Kasper A. Borup · Bo B. Iversen · Nini Pryds · Søren Linderoth

Received: 25 May 2012 / Accepted: 23 August 2012

Abstract Polycrystalline compounds of $Ca_{0.9}Y_{0.1}Mn_{1-x}Fe_xO_3$ for $0 \le x \le 0.25$ were prepared by solid-state reaction, followed by spark plasma sintering process, and their thermoelectric properties from 300 to 1200 K were systematically investigated in terms of Y and Fe co-doping at the Ca- and Mn-sites, respectively. Crystal structure refinement revealed that all the investigated samples have the O′-type orthorhombic structure, and the lattice parameters slightly increased with increasing Fe concentration, causing a crystal distortion. It was found that with increasing the content of Fe doping, the Seebeck coefficient of $Ca_{0.9}Y_{0.1}Mn_{1-x}Fe_xO_3$ tended to increase, while the tendency toward the electrical conductivity was more complicated. The highest power factor was found to be 2.1×10^{-4} W/mK^2 at 1150 K for the sample with $x = 0.05$ after annealing at 1523 K for 24 h in air. Thermal conductivity of the Fe-doped samples showed a lower value than that of the $x = 0$ sample, and the highest dimensionless figure of merit, ZT was found to be improved about 20 % for the sample with $x = 0.05$ as compared to that of the $x = 0$ sample at 1150 K.

L. T. Hung (✉) · N. V. Nong · L. Han · N. Pryds · S. Linderoth
Department of Energy Conversion and Storage, Technical University of Denmark, DTU Risø Campus, 4000 Roskilde, Denmark
e-mail: lthh@dtu.dk

D. L. Minh
Solid State Department, Faculty of Physics, Hanoi University of Science, Vietnam National University of Hanoi, Hanoi, Vietnam

K. A. Borup · B. B. Iversen
Centre for Materials Crystallography, Department of Chemistry and iNANO, University of Aarhus, 8000 Aarhus C, Denmark

Introduction

With increasing the global energy demand, thermoelectric materials have recently gained much interest in both the theoretical and technological aspects due to the potential use of these materials in converting waste heat into electricity [1, 2]. In general, for a single thermoelectric material, the conversion efficiency can be evaluated by the dimensionless figure of merit ($ZT = \sigma S^2 T/\kappa$, where σ, S, T, κ are the electrical conductivity, the Seebeck coefficient, the absolute temperature, and the thermal conductivity, respectively). The requirements for practical application of high thermal-to-electrical energy conversion place on finding suitable thermoelectric materials, and are not easily satisfied. They should not only possess good thermoelectric performance, they must also be stable at high temperatures and be composed of nontoxic and low-cost elements, but also must be able to be processed and shaped cheaply. For this purpose, metal oxide-based materials are considered as good candidates.

$CaMnO_3$, which is a perovskite oxide with orthorhombic structure at room temperature, has also been considered as a promising thermoelectric n-type material for high-temperature application [3–9]. Many attempts have been made in order to improve the thermoelectric performance of this type of material, mainly to enhance the electrical conductivity, reduce further the thermal conductivity, while avoiding degradation of the Seebeck coefficient. Most of these studies have been focused on doping, for example, Yb at Ca-site [4–7] or Nb at Mn-site [3, 8], while only few reports performed the research on dually doping, e.g., Sr and Yb at Ca-site [9]. Previous reports have showed that the substitution of Y for Ca resulted in a significant improvement in the thermoelectric performance of $Ca_{1-x}Y_xMnO_3$ system in a wide temperature region, and the

Journal : Large 10853 | Dispatch : 29-8-2012 | Pages : 6
Article No. : 6834 | LE | TYPESET
MS Code : JMSC29016 | CP | DISK

optimum doping level was found to be around $x = 0.1$ [5, 10]. Similar to other multi-valence systems such as cobaltites [11] or titanates [12], the interrelation between Mn^{3+} and Mn^{4+} should be responsible for the transport mechanism in the $CaMnO_3$ material. Therefore, doping of trivalent ions such as Fe^{3+} or Co^{3+} at the Mn-site would probably influence the transport properties of this material.

In this study, we have prepared the $Ca_{0.9}Y_{0.1}Mn_{1-x}Fe_xO_3$ system with $0 \leq x \leq 0.25$, in which Ca-site was substituted with Y at a fixed concentration and Mn-site was partly replaced by Fe. The structural and the thermoelectric properties of these set of materials were investigated in detail. The influence of Y and Fe doping at Ca- and Mn-sites, respectively, on the crystal structure was carefully studied by the Rietveld refinement analysis. The correlation between the crystal structures and the thermoelectric properties are discussed.

Experimental

Polycrystalline samples of $Ca_{0.9}Y_{0.1}Mn_{1-x}Fe_xO_3$ with $x = 0$, 0.05, 0.15, 0.2, and 0.25 were synthesized by a solid-state reaction. A mixture of commercially available $CaCO_3$ (98 %), MnO_2 (99.9 %), Fe_2O_3 (99.9 %), and Y_2O_3 (99.9 %) precursors were thoroughly mixed by ball milling with ethanol for 24 h. The mixtures were dried and then calcined at 1273 K for 24 h in air with an intermediate grinding procedure. The densify processing was carried out using a spark plasma sintering (SPS) system (SPS Syntex Inc., Japan). The samples were heated to 1123 K, while a uniaxial pressure of 50 MPa was applied for 8 min in Ar atmosphere. During the experiment, the temperature, applied pressure, and displacement of the sample were recorded continuously. The as-prepared samples were then polished in order to remove the graphite foil used during the SPS processing. The pellets were then cut into bar ($3.5 \times 3.5 \times 12$ mm^3) and plate ($10 \times 10 \times 1.4$ mm^3) shapes for the thermoelectric properties and thermal conductivity measurements, respectively. XRD analysis was carried out on the powders after calcining and after the SPS processing using a Bruker robot diffractometer with Cu-Kα radiation. Structural refinement was carried out using the Rietveld method with TOPAS 4.1. Microstructures of the samples were observed using scanning electron microscopy (SEM) with a Hitachi TM-1000 system. The electrical resistivity and the Seebeck coefficient were measured simultaneously from room temperature to 1200 K using an ULVAC-RIKO ZEM3 measurement system in a low-pressure helium atmosphere. The thermal conductivity, κ, was determined from the measured thermal diffusivity, α, the heat capacitiy, C_p, and the density, d, using the formula: $\kappa = d \times \alpha \times C_p$. The densities of the samples were measured by an AccuPyc-1340 pycnometer. The thermal diffusivity was measured by a LFA-457 laser flash system.

Results and discussion

Figure 1 shows powder X-ray diffraction (XRD) spectra measured at room temperature for pure $CaMnO_3$ and for $Ca_{0.9}Y_{0.1}Mn_{1-x}Fe_xO_3$ samples with $x = 0$, 0.05, 0.1, 0.15, 0.2, and 0.25 after they were calcined at 1273 K for 24 h in air. All the visible XRD peaks can be indexed as the pure phase of $CaMnO_3$, indicating that all the investigated samples are single phase.

Figure 2 displays XRD patterns of a typical sample with $x = 0.05$ for the calcined powder (a), spark plasma sintered pellet (b), and the SPS sample after further heat treatment at 1523 K for 24 h in air (c). As indicated by this figure regardless of heat treatment, the structure remained the same. The structure refinement for the calcined powders $Ca_{0.9}Y_{0.1}Mn_{1-x}Fe_xO_3$ system was conducted using Topas 4.1 Rietveld refinement software with input parameters which were taken from Poeppelmeier et al. [13] using space group *Pnma* (No.62), and the refined results are summarized in Table 1. The profile R value (R_p), weighted profile R-factor (R_{wp}), and Goodness of fit (GOF) values obtained in this analysis are of high quality, and is clearly illustrated in Fig. 2 for a typical $Ca_{0.9}Y_{0.1}Mn_{1-x}Fe_xO_3$ sample with $x = 0.05$ as an example. This result implies that Y and Fe most likely substituted on the Ca- and Mn-sites of $CaMnO_3$, respectively. It can be judged from the data in Table 1, that the lattice parameters follow a relation of $c/\sqrt{2} \leq a \leq b$, confirming that the polycrystalline

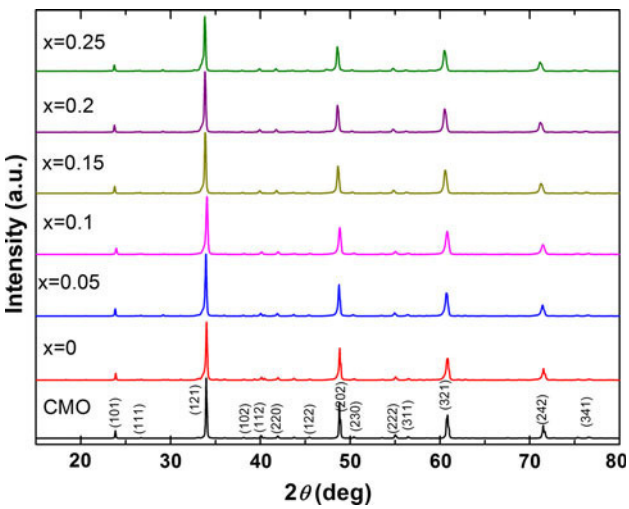

Fig. 1 XRD patterns of $CaMnO_3$ and $Ca_{0.9}Y_{0.1}Mn_{1-x}Fe_xO_3$ with $x = 0$, 0.05, 0.1, 0.15, 0.2, 0.25 samples after calcining at 1273 K for 24 h in air

Journal : Large 10853 Dispatch : 29-8-2012 Pages : 6
Article No. : 6834 LE TYPESET
MS Code : JMSC29016 CP DISK

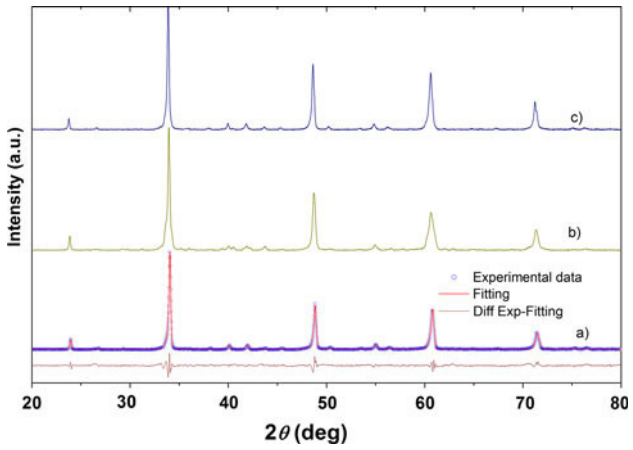

Fig. 2 XRD patterns of a typical sample $Ca_{0.9}Y_{0.1}Mn_{0.95}Fe_{0.05}O_3$: (*a*) Rietveld refinement profile of the calcined powder, (*b*) pellet sample sintered by SPS at 1173 K under pressure 50 MPa for 8 min under Ar atmosphere, (*c*) SPS sample after annealing at 1523 K in air for 24 h

compounds $Ca_{0.9}Y_{0.1}Mn_{1-x}Fe_xO_3$ of our samples have O′-type orthorhombic structure [9, 14].

The dependence of the lattice parameters and the cell volumes of $Ca_{0.9}Y_{0.1}Mn_{1-x}Fe_xO_3$ on the amount of Fe substituent are presented in Fig. 3. The result shows that the lattice parameters slightly increased with the increasing Fe concentration, resulting in an expansion in the unit cell volume. The increase in lattice parameters may be associated with the substitution of Fe^{3+} with a larger ionic radius (0.55 Å) for smaller Mn^{4+} (0.53 Å) ion [15]. In the case if Fe^{3+} substitutes for Mn^{3+} (0.58 Å), which has larger ionic radius, one would expect a slight contraction of the unit cell volume. The geometric distortion of ABO_3-type perovskites can be explained by Goldsmith tolerance factor, which is defined as

$$t = (r_A + r_O)/\sqrt{2}(r_B + r_O) \quad (1)$$

where r_A, r_B, and r_O are the ionic radii of A, B, and O atoms, respectively [15]. For $Ca_{0.9}Y_{0.1}Mn_{1-x}Fe_xO_3$ compounds, calculation of Goldsmith tolerance factors (t) showed that the highest t value was 0.988 in the case of Fe^{3+} substitutes for Mn^{4+} and the smallest t value was 0.963 with Fe^{3+} substitutes for Mn^{3+}. It implies that the orthorhombic structure is stable for all $Ca_{0.9}Y_{0.1}Mn_{1-x}Fe_xO_3$ compounds.

Figure 4 depicts the temperature dependence of the electrical conductivity for $Ca_{0.9}Y_{0.1}Mn_{1-x}Fe_xO_3$ with $x = 0$, 0.05, 0.1, 0.15, 0.2, and 0.25 spark plasma sintered samples. The result points out that the electrical conductivity of the entire samples exhibit a semiconducting-like behavior over the whole measured temperature range. However, the electrical conductivity of the spark plasma sintered samples does not show a clear tendency with the increase of Fe doping concentration. σ tends to decrease with increasing Fe concentration for $x > 0.1$, while increases for the samples with $x \leq 0.1$. It should be noted here that those samples were sintered under a high pressure at high temperature and in inert gas atmosphere. The oxygen content or even the microstructure may be varied from the samples, causing the different behaviors of the electrical conductivity as a result.

Temperature dependence of the Seebeck coefficient (S) for the spark plasma sintered samples of $Ca_{0.9}Y_{0.1}Mn_{1-x}Fe_xO_3$ with $x = 0$, 0.05, 0.1, 0.15, 0.2, and 0.25 are shown in Fig. 5. S of all investigated samples show a negative values over the whole measured temperature range, indicating n-type conduction. Contrastingly to the electrical conductivity, the absolute S values increase with increasing Fe concentration, and the effect was more substantial in low temperature region.

In order to understand further the influence of the Fe doping on the thermoelectric properties, four SPS samples with $x = 0$, 0.05, 0.1, and 0.15 were selected and further annealed at 1523 K for 24 h in air. Figure 6a shows the electrical conductivity and the Seebeck coefficient as a function of temperature after annealing at 1523 K for 24 h in air. As seen from Fig 6a, a clear tendency showing the decrease of σ, while S increases with increasing Fe concentration from $x = 0$, 0.05, 0.1 to 0.15. The value of electrical conductivity was found to increase more than two times as compared with post samples, while the Seebeck coefficient remained almost the same.

In general, the conduction mechanism of $CaMnO_3$ can be interpreted by hopping conduction [16] where hopping

Table 1 Structural refinement factors, lattice parameters, and cell volumes of $Ca_{0.9}Y_{0.1}Mn_{1-x}Fe_xO_3$

Compositions (x)	0	0.05	0.1	0.15	0.2	0.25
R_{wp} (%)	8.42	9.33	9.39	11.27	10.62	10.62
R_p (%)	6.68	6.70	6.42	7.67	7.45	6.63
GOF	1.73	1.90	1.71	1.83	1.92	1.85
a (Å)	5.28233(2)	5.27480(3)	5.3018(3)	5.3004(1)	5.29596(2)	5.29999(3)
b (Å)	7.46185(3)	7.45797(4)	7.4846(6)	7.4806(2)	7.48990(3)	7.49067(5)
c (Å)	5.26841(2)	5.27498(5)	5.2899(2)	5.3035(3)	5.28405(2)	5.28344(3)
V (Å^3)	207.659(2)	207.514(2)	209.914(2)	210.284(3)	209.598(3)	209.755(2)

Journal : Large 10853 Dispatch : 29-8-2012 Pages : 6
Article No. : 6834 LE TYPESET
MS Code : JMSC29016 CP DISK

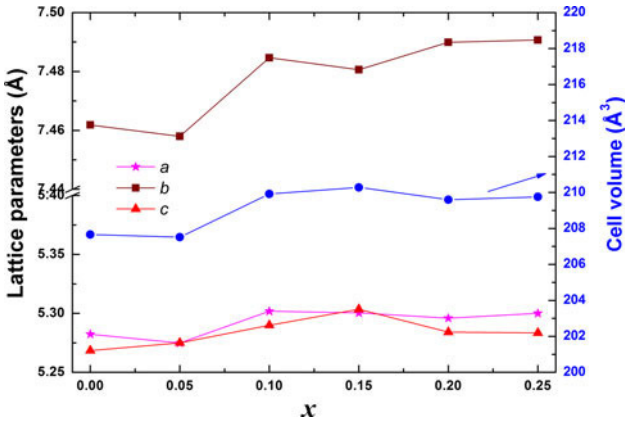

Fig. 3 Lattice parameters and cell volume of $Ca_{0.9}Y_{0.1}Mn_{1-x}Fe_xO_3$ as function of Fe content (x)

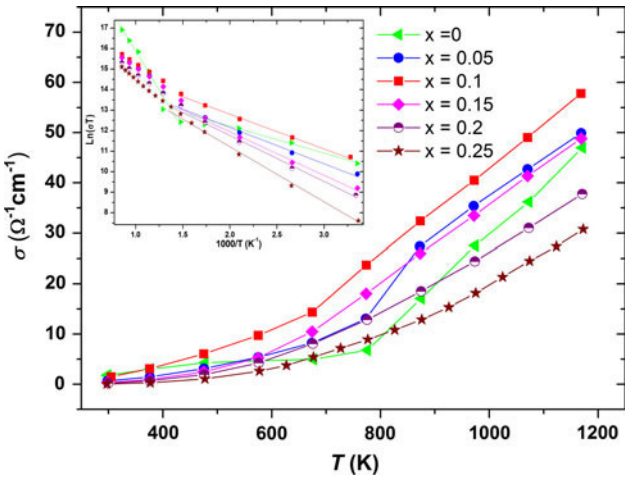

Fig. 4 Temperature dependence of the electrical conductivity for $Ca_{0.9}Y_{0.1}Mn_{1-x}Fe_xO_3$ with $x = 0$, 0.05, 0.1, 0.15, 0.2, 0.25 spark plasma sintered samples; Inset, the activation energies were fitted from experimental data

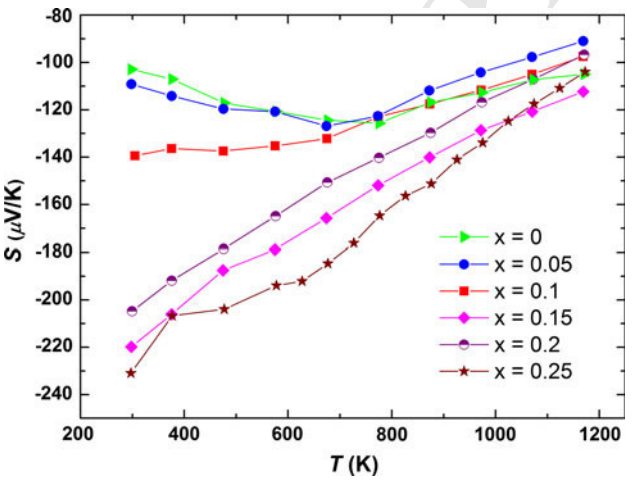

Fig. 5 Temperature dependence of the Seebeck coefficient for $Ca_{0.9}Y_{0.1}Mn_{1-x}Fe_xO_3$ with $x = 0$, 0.05, 0.1, 0.15, 0.2, and 0.25 spark plasma sintered samples

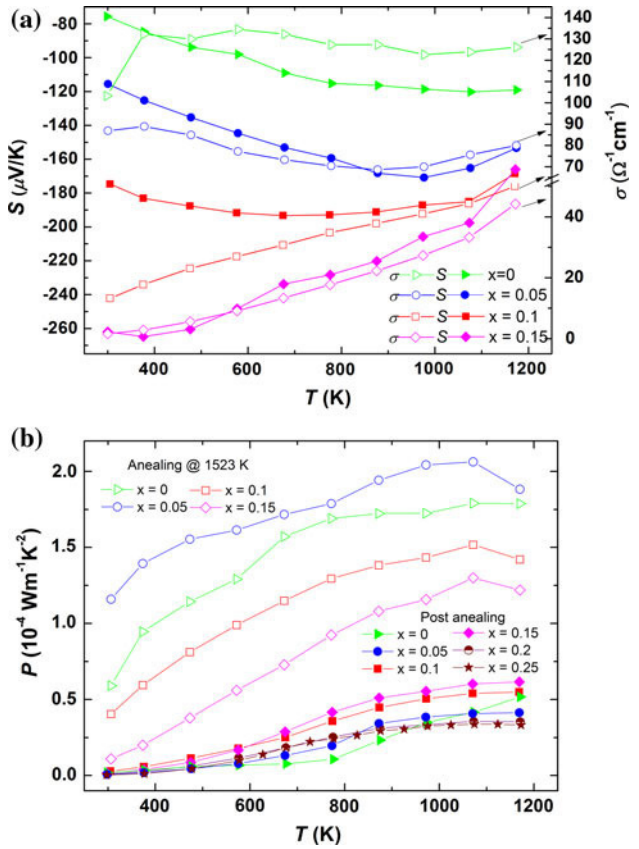

Fig. 6 Temperature dependence of **a** the Seebeck coefficient (*solid symbols*) and the electrical conductivity (*open symbols*), and **b** the PFs for all the spark plasma sintered samples $Ca_{0.9}Y_{0.1}Mn_{1-x}Fe_xO_3$ with $x = 0$, 0.05, 0.1, 0.15, 0.2, 0.25 and selective samples with $x = 0$, 0.05, 0.1, 0.15 after annealing at 1523 K for 24 h in air

of the charge carriers is thermally activated with the activation energy E_a, the temperature dependence of the electrical conductivity is given as

$$\sigma = C/T \exp(-E_a/k_B T) \quad (2)$$

where T is absolute temperature, k_B is the Boltzmann constant, and C is a constant depending on the charge carrier concentration. The activation energy could be estimated from the Arrhenius plot of LnT versus $1/T$ as shown in the inset in Fig. 4. The calculated activation energy, E_a is listed in Table 2 for all investigated samples, showing that E_a is linearly increasing with the increase of Fe substituent. However, the relationship between and E_a is only obeyed the hopping conduction's equation at temperatures below 700 K, as shown in Fig. 4 inset as well as in Table 2. As for the $x = 0$ and 0.05 samples, the LnT versus $1/T$ curve showed two different slopes in the temperature regions of $T < 700$ and $T > 700$ yielding two activate energies (see Table 2), which is similar to the observation by Vecherskii et al. [17] on the oxygen non-stoichiometry $CaMnO_{3-\delta}$ system.

Journal : Large 10853 Dispatch : 29-8-2012 Pages : 6
Article No. : 6834 LE TYPESET
MS Code : JMSC29016 CP DISK

Table 2 Relative densities and electrical characteristics of $Ca_{0.9}Y_{0.1}Mn_{1-x}Fe_xO_3$

Compositions (x)	0	0.05	0.1	0.15	0.2	0.25
Relative density (%)	94.36	94.86	97.40	96.65	95.60	93.39
E_a (meV)	117.46	146.15	155.28	181.33	189.69	227.47

For an extrinsic n-type semiconductor with negligible hole conduction, the thermoelectric power can be given by [18, 19]:

$$S(T) \approx -\frac{k_B}{e}\left[\ln\left(\frac{N_v}{n}\right) + A\right] \quad (3)$$

where e is the electric charge of the carrier, k_B the Boltzmann constant, N_V the density of states (DOS), n the carrier concentration, and A is a transport constant. Equations 2 and 3 clearly show that the decrease in carrier concentration (n) will result in an increase in the thermoelectric power (S) and vice versa. This can well explain the tendency of the Seebeck coefficient and the electrical conductivity as a function of temperature observed for the investigated samples after annealing with the increasing Fe concentration (see Fig. 6). Increasing the Fe content decreases the conductivity and increases the Seebeck coefficient which is also related to the carrier concentration via Eq. 3. However, further investigation on the carrier density and the mobility by means of the Hall measurements is currently ongoing to evidently support this interpretation.

Figure 6b shows the power factor (PF) as a function of temperature for all the spark plasma sintered samples and the selected ones after annealing. It is obvious that the PF values were remarkably improved by further heat treatment in air. The $x = 0.05$ sample showed the highest PF values over the whole measured temperature region, and the maximum PF attained was 2.1×10^{-4} W/mK^2 at about 1150 K.

To understand the reason which led to the finding interesting effect on the thermoelectric properties of the samples after heat treatment, the microstructure of the samples after SPS and after further annealing was studied using SEM, and the results are shown in Fig. 7a, b. Figure 7 shows an obvious difference in the grain size before and after the annealing. The small grains size structure observed for the spark plasma sintered sample means to be more grain boundaries, leading to the increase in electron scattering at the grain boundaries, and thus decreasing the electrical conductivity. This result well explained the behavior of the electrical conductivity for the samples before and after heat treatment.

Figure 8 shows the total thermal conductivity (κ_{total}) for all investigated samples. It can be seen that κ decreases

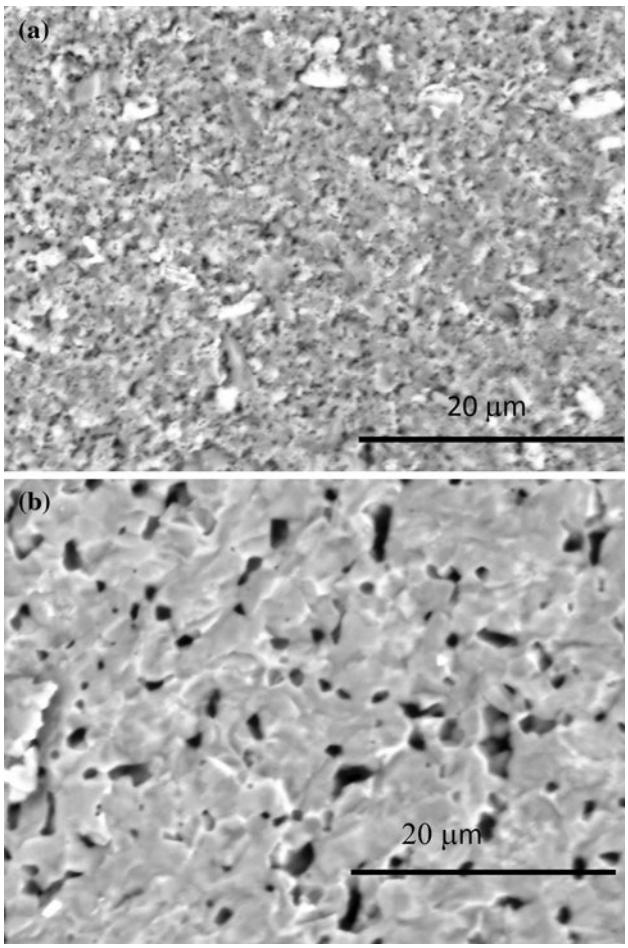

Fig. 7 SEM images from fractured surfaces of a typical $Ca_{0.9}Y_{0.1}Mn_{1-x}Fe_xO_3$ with $x = 0.05$ sample: **a** sample was sintered by SPS, **b** sample was annealed at 1523 K for 24 h in air flow

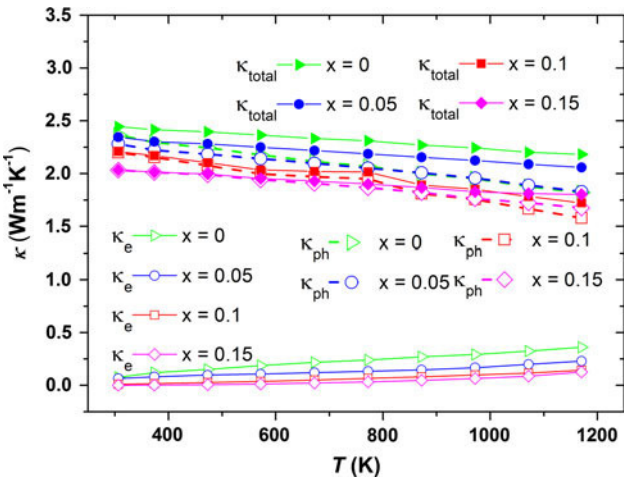

Fig. 8 the total thermal conductivity (κ_{total}), the electronic and phonon components (κ_e and κ_{ph}) of $Ca_{0.9}Y_{0.1}Mn_{1-x}Fe_xO_3$ samples with $x = 0$, 0.05, 0.1, 0.15 as a function of temperature

Journal : Large 10853 Dispatch : 29-8-2012 Pages : 6
Article No. : 6834 LE TYPESET
MS Code : JMSC29016 CP DISK

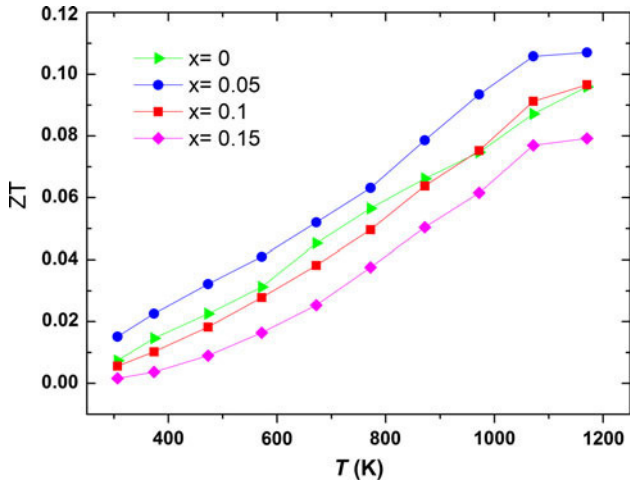

Fig. 9 The dimensionless figure of merit (ZT) as a function of temperature for $Ca_{0.9}Y_{0.1}Mn_{1-x}Fe_xO_3$ with $x = 0$, 0.05, 0.1, 0.15 selective SPS samples after heated treatment at 1523 K for 24 h in air

with increasing temperature. The substitution of Fe at Mn-sites generally decreases the thermal conductivity. The total thermal conductivity can be expressed by the sum of a lattice component (κ_{ph}) and an electronic component (κ_e), i.e., as $\kappa_{total} = \kappa_{ph} + \kappa_e$. In this case, the contribution of κ_e to κ_{total}, estimated from the Wiedemann–Franz relation, is small, indicating the major contribution of the phonon term κ_{ph}, as clearly illustrated in Fig. 8. Finally, using the measured thermoelectric data, the dimensionless figure of merit of these compositions was calculated. Figure 9 presents the dimensionless figure of merit, ZT, versus temperature for the $x = 0$, 0.05, 0.1, and 0.15 samples, showing that ZT increased for the $x = 0.05$ and then decreased again with increasing x over the whole temperature range. The maximum ZT value reached a value of 0.11 at about 1150 K for the $x = 0.05$ samples.

Conclusion

The effect of Fe substitution on the structure and the high-temperature thermoelectric properties of $Ca_{0.9}Y_{0.1}Mn_{1-x}Fe_xO_3$ ($x = 0$, 0.05, 0.1, 0.15, 0.2, 0.25) was investigated in details. Structural analysis shows that lattice parameters slightly increase with increasing amount of Fe substituent, which originates from the difference in the ionic radii between Fe and Mn ions. The thermoelectric properties were found to be improved for the Fe-doped samples with $x < 0.1$, particularly for the SPS samples with further annealing mainly due to the increase in the Seebeck coefficient that could overcome the simultaneous decrease of the electrical conductivity. The thermal conductivity was suppressed by the substitution of Fe for Mn. The maximum PF attained was 2.1×10^{-4} W/mK^2 for the $x = 0.05$ sample at 1150 K giving a maximum $ZT = 0.11$, which is about 20 % higher than the $x = 0$ sample. Further study should be performed with finer Fe substituent tuning with $x < 0.1$ in order to optimize these compounds high-temperature thermoelectric properties.

Acknowledgements The authors would like to thank the Programme Commission on Energy and Environment (EnMi) which is part of the Danish Council for Strategic Research (Contract No. 10-093971) for sponsoring this work via the OTE-POWER research work.

References

1. Rowe DM (ed) (2006) Thermoelectric handbook: macro to nano. CRC/Taylor & Francis, Boca Raton
2. Snyder GJ, Toberer ES (2008) Nat Mater 7:105
3. Bocher L, Aguirre MH, Logvinovich D, Shkabko A, Robert R, Trottmann M, Weidenkaffet A (2008) Inorg Chem 47:8077
4. Kosuga A, Urate S, Kurosaki K, Yamanaka S, Funahashi R (2008) Jpn J Appl Phys 47(8):6399
5. Wang Y, Sui FanH, Wang X, Su Y, Su W, Liu X (2009) Chem Mater 21:4653
6. Flahaut D, Mihara T, Funahashi R, Nabeshima N, Lee L, Ohta H, Koumoto K (2006) J Appl Phys 100:084911
7. Wang Y, Sui Y, Su W (2008) J Appl Phys 104:093703
8. Bocher L, Aguirre MH, Robert R, Logvinovich D, Bakardjieva S, Hejtmanek J, Weidenkaff A (2009) Acta Mater 57:5667
9. Kosuga A, Isse Y, Wang Y, Koumoto K, Funahashi R (2009) J Appl Phys 105:093717
10. Thuy NT, Minh DL, Nong NV, Bahl CRH and Pryds N, 7-9 November, Ho Chi Minh city, Vietnam (2011), Proceedings of the solid state physics and materials science symposium (in press)
11. Nong NV, Pryds N, Linderoth S, Ohtaki M (2011) J Adv Mater 23(21):2484
12. Wang HC, Wang CL, Su WB, Liu J, Sun Y, Peng H, Mei LM (2011) J Am Ceram Soc 94(3):838
13. Poeppelmeier KR, Leonowicz ME, Scanlon JC, Longo JM (1982) J Solid State Chem 45:71
14. Kostogloudis GC, Fertis P, Ftikos C (1999) Solid State Ionics 118:241
15. Shanon RD (1976) Acta Crystallogr A A32:751
16. Karim DP, Aldred AT (1979) Phys Rev B 20:2255
17. Vecherskii SI, Konopel'ko MA, Esina NO and Batalov NN (2002) Inorg Mater 38(12):1491
18. Jonker GH (1968) Philips Res Rep 23:131
19. Ohtaki M, Tsubota T, Eguchi K, Arai H (1996) J Appl Phys 79:1816

Journal : Large 10853 | Dispatch : 29-8-2012 | Pages : 6
Article No. : 6834 | LE | TYPESET
MS Code : JMSC29016 | CP | DISK